CBN 99-23

Mechanical Analysis of Stresses in Superconducting Interaction Region Magnets for CESR Phase III

James J. Welch

August 11, 1999

Contents

1 Introduction

When completed the phase III upgrade of CESR will include new short focal length high gradient superconducting magnets in the interaction region. The topic of this paper is rather narrow and covers only the analysis of the internal thermally induced mechanical stresses in the magnets. The subjects of electromagnetic forces and the phase III upgrade are covered in [1], [2], and [3].

Thermally induced stresses are critically important because the superconducting state is easily lost if there are any internally dissipative motions that cause local heating or movement of the conductor. When the magnet is energized the induced electromagnetic forces are quite large. To prevent dissipative motions the magnets are pre-loaded with initial stresses substantially larger than the changing electromagnetically induced stresses. The pre-load locks all the parts of the magnet together into one mechanical state resulting in much stronger and stiffer object. In the case of the Cornell superconducting magnets the pre-load is supplied using aluminum shrink rings. Because aluminum shrinks more than the other coil materials, when cooled the rings squeeze down radially on the assembly of coils causing large radial and azimuthal stresses. [1]

There is a single parameter that has the greatest effect on the pre-load obtained and that is the room temperature interference fit between the aluminum shrink rings and the magnet. There is relatively little variability in the possible coil materials or sizes . Likewise the overall thickness of the ring is more or less fixed by the available space. However if the inteference fit is too loose by a few tenths of a millimeter little or no pre-load will result, if too tight the stresses may get so high that insultation is damaged.

To determine a best value for the interference fit I used a finite element model to estimate the pre-load stresses as a function of interference fit. To output of the model is critically dependent on simplifying assumptions, and especially on the choice of materials properties. To this end I have obtained several sources of information about the material properties, including some actual direct measurements made on various magnet assemblies.

2 Materials and their Properties

The magnets are composed on many heterogenous and anisotropic materials whose properties depend critically on temperature. Individual material properties can be found in the literature, though there is considerable spread in some of the quoted values, especially for non-metals. More information can be obtained by direct measurement on the magnets at room temperature. To use this

[1] Some longitudinal pre-load may also be present at room temperature mainly from the winding tension. More will likely be generated by the differential contraction during cooldown, however, in the Cornell design it will be highly non-uniform and not accumulate because the aluminum shrink rings are divided into four separate pieces. Even less significant are stresses due to forces borne by the magnet through the support points to the cryostat. Support forces need only be strong enough to react the net forces and moments on the magnet body and there are a lot of internal cancelations. See Appendix.

information I developed some averaging procedures and an analytic model of the magnet and shrink ring which depends only on the average moduli of the materials.

2.1 Magnet Composition

The main components of the Cornell magnets are shown in Figure 1. The shrink ring is made of 7075 Al, the coil blocks are composites of superconducting wire (itself a composite of NbTi and copper), kapton insulation and tiny voids mostly filled with epoxy resin. There are thin but significant spacers made out of fiberglass sheet which are used to shim the coil sizes. Between coil blocks are long spacers made of either copper and stainless steel. In the coil ends are complex castings made of phosphor bronze which guide the wire as it makes its was from one turn to the next. Also in the ends are innumerable small pieces of G-10 and kapton that fill various odd voids due to joggles and other winding details.

2.2 Material Properties

Relevent material properties include thermal expansion, elastic moduli, and strength or usable2 usable usable stress limits. These properties were obtained for room temperature and liquid helium temperature. For aluminum, which is heated for the shrink fit, the thermal expansion above room temperature was also obtained.

Aluminum shrink rings provide the driving force to obtain pre-load on the magnet. Both the contraction and the elastic modulus of aluminum are well known and the uncertainties are essentially irrelevant irrelevant. The same can be said of the stainless steel central post and the copper spacers. For these materials I use numbers provided by Zlobin, [4] but checked against other sources. Except for aluminum, the assumed data can be found in Table 1.

Other materials used in the magnets: superconducting wire, kapton insulation, fiberglass spacers, nomex, epoxy, epoxy impregnated glass banding, and to some extent the effect of small voids in the coil assembly, are largely anisotropic and vary in properties from one sample to another depending on the curing temperature, or percentage of glass, etc. Because of the inherent uncertainty, I did not try to model the anisotropy directly but instead analyzed cases with the minimum and maximum values without regard to direction.

One of the more important components are the coil blocks. In reality they are heterogeneous composites of superconducting wire with kapton insulation, all bonded together by epoxy impregnation. There are three different type of coil blocks: main quadrupole, skew quadrupole and dipole. For the finite element analysis each type of coil block was represented as a uniform material whose material properties were chosen to be a properly weighted average of the component material properties. For the analytic calculation the different coils were suitably averaged all together to form an estimate a generic coil material.

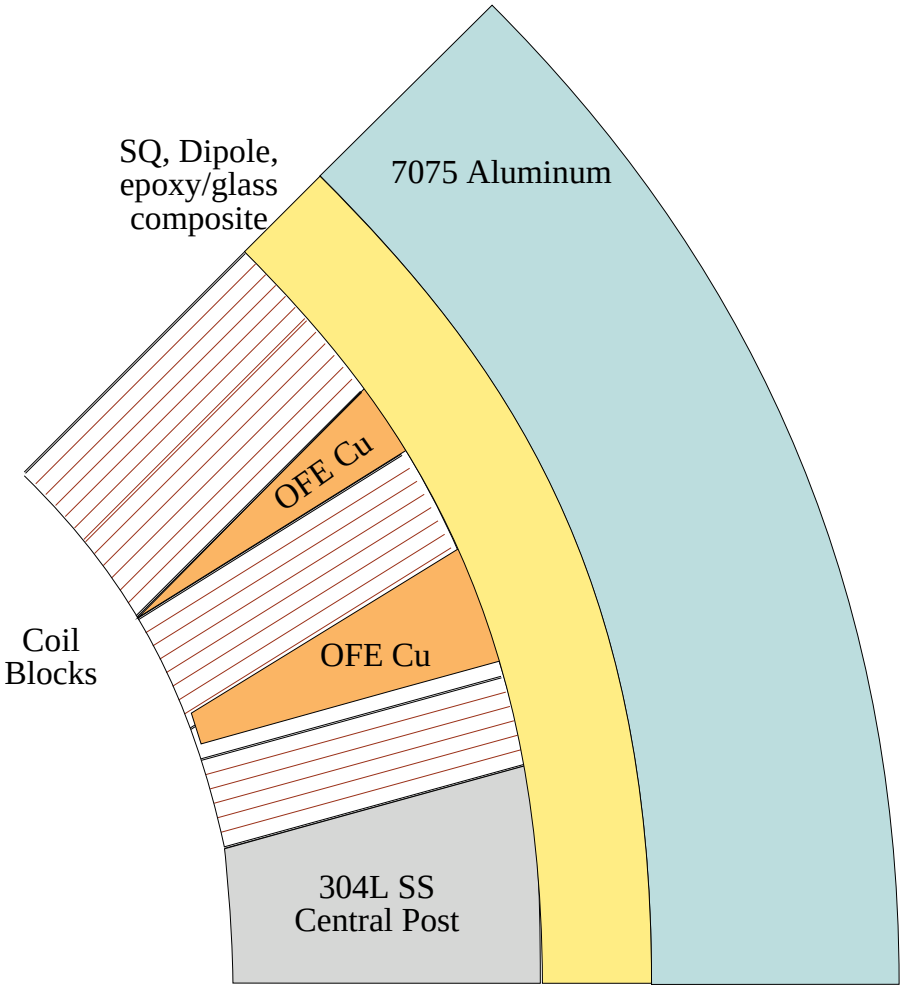

Figure 1: Basic components used in models of the prototype magnet are shown in the one-eighth slice of a cross section of the prototype magnet.

A table summarizing the coil material properties assumed in the finite element model is given in Table 1.

The averaging method to obtain the net modulus of a coil block was as follows. For a sandwich of different materials, each of thickness L_i and elastic modulus E_i, the net modulus is calculated as:

$$\frac{L_{net}}{E_{net}} = \sum_i \frac{L_i}{E_i} \tag{1}$$

If the components are in parallel the net effect is calculated from:

$$E_{net}\ \text{Area}_{net} = \sum_i E_i\ \text{Area}_i \tag{2}$$

To get the effective contraction coefficient for a composite material I used an analogous set of equations. Because the wire is not square, but the kapton around it is uniformly thick the coil blocks should in reality behave somewhat anisotropically. However in the model I assumed isotropic materials and used values for the moduli that were the average of the anisotropic values.

This method of averaging materials properties shows that ven though kapton (and other plastics for that matter) may only be a small percentage coil thickness, its low modulus contributes substantially to the overall average coil modulus.

2.3 Measurements of the potted coil

A analytical laboratory was contracted to perform modulus measurement of a section of potted MQ coil at room temperature and at liquid nitrogen temperature. The results are quoted in table 2. The measured coil seems to be in the range of values based on averaging and publish measurements for room temperature and at the stiff end of the range for moduli when cold (see Table 1).

2.3.1 Modulus measurements

Measurements were made of the room temperature average magnet modulus on the assembly of four main quadrupole coils and banding which is referred to as the 'Four Coil Assembly'. This assembly differs from the prototype and other magnets only in that the skew quadrupole and dipole coils are replaced by additional banding. Additional measurements were carried out on the prototype and the unit assemblies. In all cases a special heavy steel clamping structure was made which could uniformly clamp down on the assembled magnet coils with a varying degree of pressure as shown in Figure 2. A large micrometer was then used to measure the diameter change of the magnet as a function of the load. The bolt force was assumed to be related to the torque by $F_{bolt} = 5T/\phi^2$ and the torque was measured with a torque wrench. The bolt tension must

[2]Recommended by a British mechanical handbook and others as being ±25% good.

Table 1: Minimum, maximum and average moduli used in the finite element model.

Prototype		**E @ RT**			**E @4.6K**		
	Size	**[Gpa]**			**[Gpa]**		
	mm	**low**	**ave**	**high**	**low**	**ave**	**high**
Azimuthal average							
Central post	23	190	190	190	210	210	210
potted coil	50	25	31	37	55	72	84
copper spacers	14.3	120	120	120	135	135	135
net MQ composite	87	39	47	54	78	96	108
Radial average							
MQ composite	40	39	47	54	78	96	108
SQ/D composite	14	6	7	9	11	15	19
net Coil Modulus	53	**30**	**37**	**43**	**61**	**76**	**85**

Four Coil Assembly		**E @ RT**			**E @4.6K**		
	Size	**[Gpa]**			**[Gpa]**		
	mm	**low**	**ave**	**high**	**low**	**ave**	**high**
Azimuthal average							
Central post	25	190	190	190	210	210	210
potted coil	48	25	31	37	55	72	84
copper spacers	25	120	120	120	135	135	135
net MQ composite	98	39	47	54	78	96	108
radial average							
MQ composite	40	39	47	54	78	96	108
pure banding	11.0	8	10	12	14	21	27
net Ave. Coil Modulus	51	**31**	**38**	**44**	**61**	**77**	**87**

Table 2: Laboratory measurements of a section of potted coil.

	Room Temp. [GPa]	LN Temp. [GPa]
Modulus (azimuthal)	22 - 25	83-98

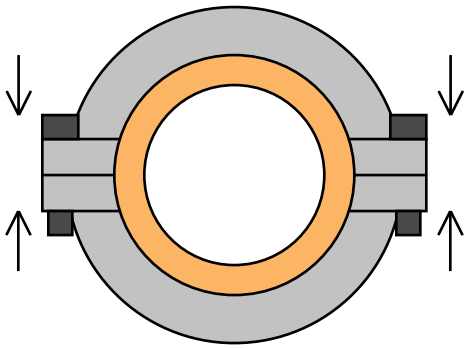

Figure 2: Schematic of collar and magnet during modulus test.

be reacted by the average azimuthal stress in the coil. The average azimuthal stress is therefore the total bolt force divided by the coil cross-sectional area.

Measurements were made with the modulus tester placed in the middle of the coil assemblies, and at one end of the assemblies. While the tester was in the middle there were two measurements made, one where the diameter was measured at the stainless steel central post, and the other where the diameter was measured on the banding. Figure 3 shows the results of the measurements for the four coil assembly. Series 3 and series 6 are most relevant as the stress levels there are the highest. They indicate that there is an offset at zero stress of about 30-50 μm which may be accounted for by surface texture, or perhaps static bolt friction. Series 3 shows the change in the diameter in the middle of the magnet measured directly on the central post, while series 6 shows the diameter change at the end of the magnet. The peak applied azimuthal stress was about 30 MPa.

2.3.2 Analysis of modulus measurements

Measurements were also carried out on the prototype assembly and the unit 2 assembly. To determine the effective average modulus I used an analytic model described in Section 3.1. In this model, the modulus was varied until the observed ratio of theoretical diameter change to applied azimuthal stress matched the measured ratio, as determined from a straight line fit to the diameter data. Based on the analytic model and the modulus measurement, the effective elastic moduli at room temperature are determined. They are given in the Table 3.

The modulus measurements indicate there is a substantial modulus difference between the middle and the ends of the magnet, which is not surprising. The ends contain large phosphor bronze castings that are hand fitted to the complex coil geometry. Small odd-shaped volumes are formed in the ends when the wire is joggled from one layer to another and these volumes are filled with hand made G-10 spacers. There is also much more kapton in the ends as a thick

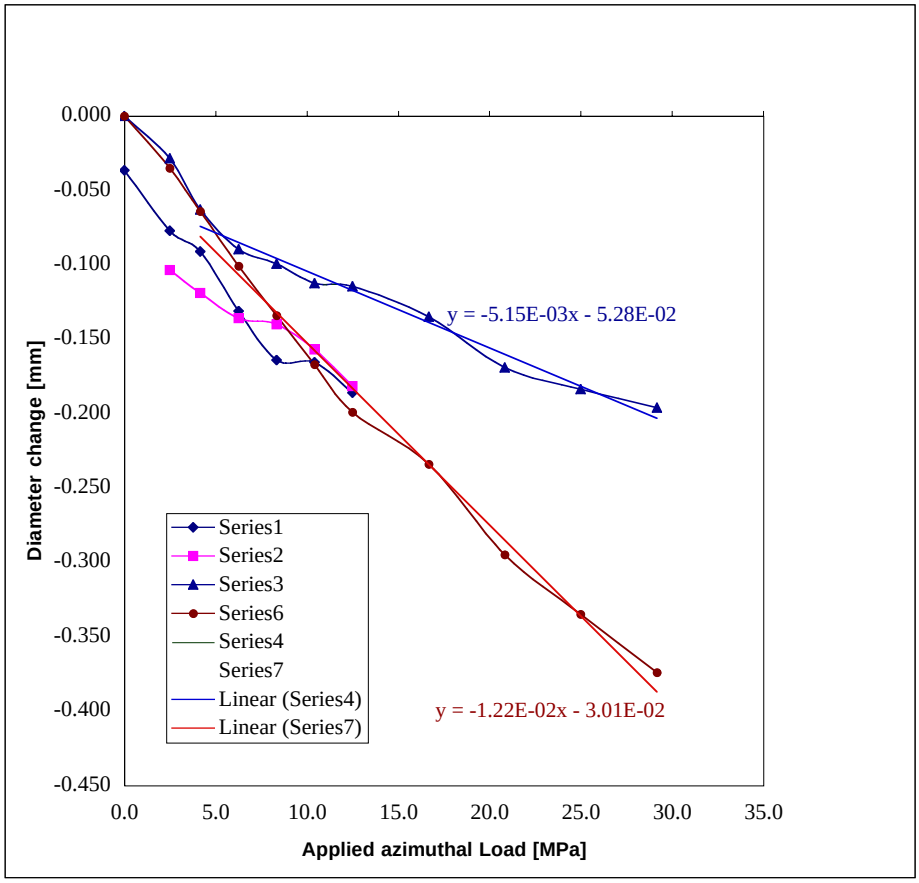

Figure 3: Results from modulus test.

Table 3: Estimated elastic modulus based on the analytic model and the modulus measurement test.

	Eff. Modulus at 20°C [GPa]	
Measurement	Middle	End
Four Coil	42	18
Prototype	25	12
Unit 2	30	14
Average	32	15

sheet is put between each layer of windings. Overall the presence of a greater amount of low modulus materials and small voids make it understandable that the effective modulus in the ends is lower than in the middle of the magnet.

It is interesting to jump ahead and compare the analytic model estimates of the average magnet modulus with prediction of the finite element model based published values and various averaging techniques. At room temperature the finite element model indicates the average coil modulus is in the range from 31 to 44 GPa with an average of 38 GPa depending on the spread in published data. The average analytic model estimate for the middle is 32 GPa which is on the soft end of the range but in agreement. On the other hand the ends would appear to be half a soft as the minimum considered in the finite element model.

Another consideration that should be taken into account is that the analysis of the modulus measurement (see section 3.1) assumed an infinite length tester and magnet while in reality the tester is short compared with the length of the magnet. The effect of this is that magnet outside of the tester acts to strengthen the part of the magnet inside the tester and results in a higher modulus estimate than is real. The magnitude of this effect was estimated by making another finite element model of the modulus measurement itself, which included the full three dimensional geometry. It turns out that the effect is small. The artificial enhancement of the modulus is only 12% for the measurement of the middle of the magnet and about half that for the end measurement. If this correction is applied to the estimates we have an average of 29 MPa for the middle and 14 MPa for the ends.

3 Methods of Analysis

Two independent methods of analysis were developed to estimate the stress levels at various temperatures for different interference fits: analytic and finite element. The analytic method is based on approximating the magnet as two concentric rings of uniform (but different) materials. It is simple and reasonably accurate provided suitable average ring material properties can be found. It is especially useful in checking assumptions against modulus measurements of the actual magnet. However it is not easy to extent this model to low temperature, nor is it possible to see in detail how the stresses may be distributed within the coil structure. The finite element model includes the detailed shapes of the coils and spacers, though not in a full three dimensional form, and the material properties are modeled as temperature dependent.

3.1 Analytic

The analytic estimate was developed based on formulae in Roark, page 638 table 32 1a and 1c, for a uniformly radially loaded thick circular cylinder. For a given radial stress on the outside of a thick cylinder, formula 1a gives the deflection of inner and outer diameters. Formula 1c gives the deflection if the load is on the inside of the cylinder. The aluminum shrink ring is represented by an internally

radially loaded cylinder and the magnet coils by an externally radially loaded coil. The maximum stress within each ring occurs at the inner radius.

The net radial load at the interface, q, must be equal and opposite for the coils and the aluminum when the aluminum is shrunk around the magnet coils. This load can be eliminated algebraically in favor of the maximum azimuthal stress on inner radius of the magnet, which is defined here as σ^*. If a/b refer to the outside/inside radius and subscripts m/r refer to the magnet coils / shrink ring, then the change in inner radius of the shrink ring and Δb_r, and the change in outside radius of the magnet coils Δa_m can be derived from the formula as such,

$$\Delta a_m = \frac{\sigma^*(a_m^2 - b_m^2)}{2a_m^2}\frac{a_m}{E_m}\left(\frac{a_m^2 + b_m^2}{a_m^2 - b_m^2} - \nu\right) \tag{3}$$

$$\Delta b_r = \frac{\sigma^*(a_m^2 - b_m^2)}{2a_m^2}\frac{b_r}{E_r}\left(\frac{a_r^2 + b_r^2}{a_r^2 - b_r^2} + \nu\right) \tag{4}$$

$$\tag{5}$$

where ν is the poisson ratio and E is the modulus of elasticity.

The diametral interference fit is

$$f = 2|\Delta b_r| + 2|\Delta a_m| \tag{6}$$

This is arrived at by assuming the radial stress needed to enlarge the ID of shrink ring by Δb_r is equal and opposite to the radial pressure needed compress the OD of the magnet Δa.

Where possible I have verified that the output of the analytic model agrees with a similar model constructed previously by Albert Ijspeert.

3.2 Finite Element

Several ANSYS finite element models were created to describe both the thermal and mechanical behavior. There are three relevant temperatures: the contact temperature at which the aluminum shrink ring ID is exactly the same size as the OD of the magnet coils, room temperature at which measurements are typically done, and 4.6°K. The shrink ring is heated and slipped over the room temperature magnet. When the shrink ring cools to the contact temperature there is no mechanical strain on either the shrink ring or the magnet, yet they are in intimate contact. As the ring cools the thermal contraction generates mechanical stress which is borne by both the magnet and the ring. Eventually the assembly reaches room temperature. This is the state of the model when results are quoted at room temperature. The assembly is then cooled to liquid helium temperature. In this process only the difference in the contraction of the ring and the magnet can generate mechanical stress. Because the ring contracts more than the magnet the stress levels increase as the temperature is lowered.

One peculiarity that deserves mention is the way the contraction data is supplied to ANSYS. ANSYS only accepts thermal contraction information in

the form of a temperature coefficient. For ANSYS to calculate the actual thermal contraction it needs the temperature and *the reference temperature* at which zero strain is assumed. For constant contraction coefficient this would present no complication, but in our case the contraction is decidedly non-linear with temperature. Consequently a different value for the contraction coefficients must be supplied whenever the reference temperature is changed. The reference temperature i.e., the contact temperature, must be changed every time a different interference fit is to be evaluated.

ANSYS can present a plethora of information about the mechanical state of the model. For simplicity I will refer only to the von Missus stress and the overall change in size. To avoid damage to the kapton in particular, it was recommended to keep the von Missus stress less than 80 MPa on the coil block; the damage threshold for kapton at liquid helium temperature is estimated at 140 MPa [4]. The other materials are much stronger and are not likely to be damage. Electromagnetic forces will add and subtract from the pre-load. To avoid coil motion and consequent quench the Lorentz induced stresses should be always and everwhere less than the pre-load stresses and having the pre-load near the maximum tolerable value. The maximum size of the electromagnetic stress are expected to be substantially less than the desired pre-load stress.

4 Analysis Results

After many iterations involving changes in material properties and different interference fits I arrived at a 'good' set of values which produce appropriate amounts of pre-load. That ideal theoretical fit is 0.28 mm diametral interference measured at room temperature, which is equivalent to a contact temperature of 60°C.

4.1 von Missus stress

According to the finite element model this fit generates von Missus stress in the main quad coil blocks up to a peak value of about 82 MPa at liquid helium temperature. The von Missus stresses are plotted in Figure 4. At room temperature the peak stress is about 27 MPa. See Table 4 for a synopsis of the stress results. The minimum and maximum correspond to different azimuthal location. The average is simply the average of the minimum and maximum.

4.2 Geometric distortions

The diameter changes of the magnet and shrink ring at room temperature and at liquid helium temperature are given in the Table 5. Considerable care must be taken in understanding just exactly what diameter is measured or estimated. If the aluminum rings are machined to a certain OD measured at room temperature, when they are raised to the contact temperature the OD will have grown. ANSYS models the coil/shrink ring assembly from this point on and calculates

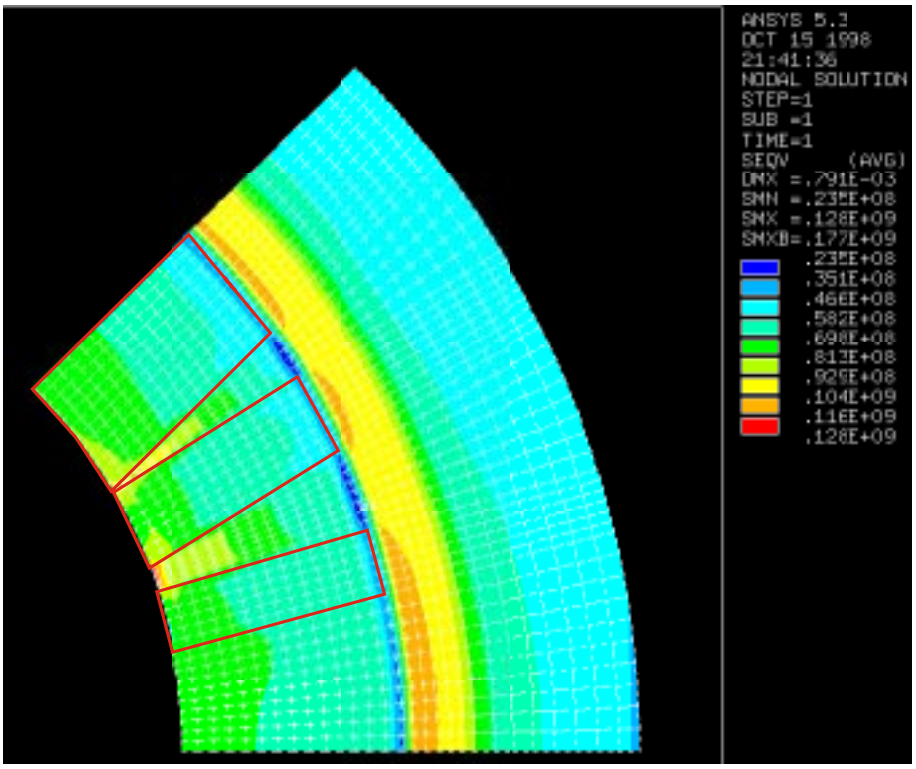

Figure 4: Von Misses stress for the prototype magnet unit at liquid helium temperature. A 60 °C contact temperature is assumed.

Table 4: Maximum Von Missus stress on the coil for different temperatures and assumptions about material properties based on the finite element model. These data assume the contact temperature of 60 °C. The MQ azimuthal stress is actually taken from the inner radius of the coil just at the central post but almost the same as values in the coil blocks.

	Max MQ Stress [MPa]	Max SQ/D Stress [MPa]	Ave Azi. MQ Stress [MPa]
Ave Properties			
Room Temperature	27	7	24
4.6 °K	82	112	73
Soft Material Properties			
Room Temperature	24	6	22
4.6 °K	71	95	62
Stiff Material Properties			
Room Temperature	28	7	26
4.6 °K	85	106	78

the change in the size of the ring as it cools from the contact temperature and is experiencing stresses. At room temperature the coil assembly tends to keep the ring from shrinking back to its original size so a actual measurement of the ring diameter after it cools to room temperature should show an increase. As far as ANSYS is concerned the coil was at its original size when it was at the defference contact temperature and at room temperature has decreased it size. The between the ANSYS estimate and the actual size is exactly equal to the expansion of the ring OD from room temperature to the contact temperature. We have

$$\Delta\phi_{actual} = \alpha\Delta T \times OD - \Delta\phi_{ANSYS} \tag{7}$$

The actual diameter change of the shrink ring is given in Table 5 assuming a contact temperture of 60 °C and room temperature of 20 °C. This corresponds to an expansion of the OD of the shrink ring of 330 μm.

5 Interference Fit

The desired interference fit must take into account the desired stress levels, practical limitations of measurement, and variation, uncertainty and incomplete understanding of the material properties.

The desired stress levels are given in Table 4. Depending on the actual material properties one can expect the highest stress point in the coil not to

Table 5: Estimated OD changes of the shrink rings based on the finite element analysis. Diameter were determined separately at the central post (CP) and the coil edge. The contact temperature of 60 °C.

	$\Delta\phi_{net}$ at CP [μm]	$\Delta\phi_{net}$ coil edge [μm]	$\Delta\phi_{net}$ average [μm]
Average Material Properties			
Room Temperature	+147	+162	+154
4.6 °K	−1252	−1234	−1243
Soft Material Properties			
Room Temperature	+131	+147	+139
4.6 °K	−1266	−1244	−1255
Stiff Material Properties			
Room Temperature	+152	+165	+159
4.6 °K	−1245	−1230	−1237

exceed 112 MPa but be greater than 71 MPa (cold). The upper limit of this range is somewhat higher than the recommended maximum of 80 MPa. Several factors argue that the chosen interference should be larger than theoretical desired value: experience with the Q09 magnets, softer ends than middle, the possibility of yielding when the hot shrink rings are put on the banding, the fact that the actual failure stress of the kapton is considerably above 80 MPa, and the fuzz effect all help to subjectively push to a tighter interference fit.

The fuzz effect, (see Section 2.3.1), whereby the measured OD appears to be about 50 μm larger than the effective OD, indicates the measured interference should be increased by this amount above the theoretical. It would seem plausible that the ID measurement might also be subject to this effect.

The softer ends would probably be optimally loaded with a tighter fit, but no adequate 3D model has been developed to see whether the stress enhancements on the coil are more or less than in the middle of the magnet. This might be an avenue to pursue if the quench performance is not sufficient.

In summary the desired inteference fit is derived from the 60 °C contact temperature for which the stress estimates are given in Table 4. A contact temperature of 60 °C is equivalent to an effective diametral interference of 0.299 mm. The measured diameter should be bigger by the fuzz amount. I will include a hypothetical ID fuzz on the aluminum shrink ring of 0.06 mm to further bias the fit toward tightness. The net result is: *the desired measured diametral interference fit at room temperature is* 0.419 *mm.*

In actual practice the room temperature stress levels can be checked after the shrink fit has been applied by measuring the increase in the shrink ring diameter. This was done for three case and the results are summarized in Table 5. The

Table 6: Ratio of measured room temperature stress to estimated stress based on the modulus measurement and the analytic model.

Assembly	Middle	End
Four coil	0.29	0.41
Prototype	0.60	0.53
Unit 2	0.70	1.03
Unit 3	0.65	0.66

stress is directly proportional to the diameter increase of the shrink ring after fitting.

There was relatively little pre-load obtained in the four coil assembly. Subsequent fitting operation avoided the use of shrink rings at temperatures above $120°C$ as it was felt that yielding of the banding had occured when the hot shrink ring $> 150°C$ was placed on the magnet. There is still considerable variation in apparent room temperature stress levels, as well as a marked tendancy for the stress levels to be less than the theoretical. This latter feature is partially explained by the 3D effect in the determination on the modulus, but only accounts for a 12% in the middle and 6% in the ends. The remaining discrepancy is not understood.

A Longitudinal Stresses

The central post, copper spacers and conductor each form long parallel elements which will differentially contract longitudinal. The aluminum shrink rings, however are made of four equal length sections so there contraction affects the coil mass only locally. Winding tension puts the central post in compression during winding. However when the coil is released from the former it is not clear how much if any winding tension remains. The electromagnetic forces on the ends of the quadrupole windings generate very large longitudinal forces trying to pull the magnet apart. These are generated in the conductor and transferred to the other components of the magnet. Forces on the magnet due to the support system are only transverse.

A.1 Winding Tension

The winding tension is graded starting with highest tension for the innermost layers. Grading the tension help prevent loosening of the innermost turns as additional turns are put on. The program of tension is given in Table 7. The wire has been tensile tested at room temperature to break at 7.9% elongation and 680 MPa.

Table 7: Winding tension program for the Cornell phase III interaction region magnets.

	Tension [N]	Stress [MPa](ksi)
Block 1	370	79 (12)
Block 2	275	59 (8)
Block 3	240	51 (7)

A.2 Contraction Stresses

The estimated contractions at liquid helium temperature is given in the table Iduuno. What does this mean.

A.3 Electromagnetic Longitudinal Stresses

Electromagnetic forces are generated by the interaction of the current in the ends of main quadrupole windings and the field that the magnet produces. At full operating current (1225 A) there will be 3.5×10^5 N tension pulling out each end of the magnet. If all this tension was carried by the windings it would generate an average tensile stress in the windings of 102 MPa, which is comparable and somewhat larger than the winding tension. Near the end of the straight section this may be near the actual case, but in the middle of the straight section the central post and straight spacers should carry much of the tensile load. Hence 102 MPa is perhaps representative of the upper limit of electromagnetic induce tension in the wire which might be approached at the junction between the straight section and the end of the coil. When the magnet is de-energized the tension is removed.

References

[1] J.J. Welch and G.F. Dugan *Forces on Interaction Region Quadrupoles and-Dipoles Due to a Detector Solenoid Magnet, (PAC97)*

[2] J.J.Welch, G.F. Dugan, E. Nordberg, D. Rice, Cornell University, *The Superconducting Interaction Region Magnet System for the CESR Phase III Upgrade*, (PAC97)

[3] S.D. Henderson and J.J. Welch, et. al. *CESR Phase III Interaction Region* (PAC99)

[4] Taken from material contributed by A. Zlobin to the Final Design Review, available from J. Welch (1997)